

Effect of Grain Shape and Relative Humidity on the Nonlinear Elastic Properties of Granular Media

Linying Gao¹, Parisa Shokouhi², and Jacques Rivière²

¹The Pennsylvania State University

²Pennsylvania State University

January 3, 2023

Abstract

This study focuses on unraveling the microphysical origins of the nonlinear elastic effects, which are pervasive in the Earth's crust. Here, we examine the influence of grain shape and relative humidity (RH) on the elastic nonlinearity of granular assemblies made of spherical glass beads and angular sand particles. We find that their elastic nonlinearity is of the same order of magnitude. However, while the elastic nonlinearity of glass beads increases with RH, that of sand particles is rather RH independent. We attribute this difference to the angularity of sand particles; absorbed water on the spherical grains weakens the junctions making them more nonlinear, while no such effect occurs in sand due to grain interlocking. Additionally, for one of the nonlinear parameters that likely arises from shearing/partial slip of the grain junctions, we observe a sharp amplitude threshold in sand which is not observed in glass beads.

Hosted file

951593_0_art_file_10513731_rm3685.docx available at <https://authorea.com/users/564380/articles/611241-effect-of-grain-shape-and-relative-humidity-on-the-nonlinear-elastic-properties-of-granular-media>

Hosted file

951593_0_supp_10512859_rmhryy.docx available at <https://authorea.com/users/564380/articles/611241-effect-of-grain-shape-and-relative-humidity-on-the-nonlinear-elastic-properties-of-granular-media>

1 **Effect of Grain Shape and Relative Humidity on the Nonlinear Elastic Properties of**
2 **Granular Media**

3 **L. Gao¹, P. Shokouhi¹, and J. Rivière¹**

4 ¹ Department of Engineering Science and Mechanics, Pennsylvania State University, University
5 Park, Pennsylvania 16802, USA.

6 Corresponding author: Linying Gao(lzg245@psu.edu)

7 **Key Points:**

- 8 • The elastic nonlinearity of spherical particles increases with relative humidity increase,
9 while it is rather constant in angular particles.
- 10 • We attribute this RH independence in sand to grain interlocking that prevents adsorbed
11 water from weakening the grain junctions.
- 12 • For angular particles, we observe an amplitude threshold above which grain junctions
13 start to unlock and where sliding/partial slip occurs.
14

15 **Abstract**

16 This study focuses on unraveling the microphysical origins of the nonlinear elastic effects, which
17 are pervasive in the Earth's crust. Here, we examine the influence of grain shape and relative
18 humidity (RH) on the elastic nonlinearity of granular assemblies made of spherical glass beads
19 and angular sand particles. We find that their elastic nonlinearity is of the same order of
20 magnitude. However, while the elastic nonlinearity of glass beads increases with RH, that of
21 sand particles is rather RH independent. We attribute this difference to the angularity of sand
22 particles; absorbed water on the spherical grains weakens the junctions making them more
23 nonlinear, while no such effect occurs in sand due to grain interlocking. Additionally, for one of
24 the nonlinear parameters that likely arises from shearing/partial slip of the grain junctions, we
25 observe a sharp amplitude threshold in sand which is not observed in glass beads.

26

27 **1 Introduction**

28 Nonlinear elastic effects arise in solids due to the presence of imperfections at the
29 micro/mesoscopic scale, such as cracks or dislocations (Ostrovsky & Johnson, 2001).
30 Understanding the origins of these nonlinear elastic effects is critical to numerous fields, from
31 geophysics (Abeelee et al., 2002; Delorey et al., 2021; Feng et al., 2018, 2022; Guyer & Johnson,
32 2009; Hillers et al., 2015; P. Johnson & Sutin, 2005; Manogharan et al., 2021; McCall & Guyer,
33 1994; Shokouhi et al., 2020; Tadavani et al., 2020; TenCate et al., 1996, 1996, 2016) and civil
34 engineering (Abeelee & De Visscher, 2000; Astorga et al., 2018; Bittner & Popovics, 2022; G.
35 Kim et al., 2017; Lacouture et al., 2003; Payan et al., 2014; Shokouhi et al., 2017) to the non-
36 destructive evaluation of materials (Breazeale & Ford, 1965; Buck et al., 1978; Jin et al., 2020;
37 J.-Y. Kim et al., 2006; Matlack et al., 2015; Williams et al., 2022). Elastic nonlinearity is
38 particularly large in poorly consolidated or unconsolidated materials, where it arises from weak
39 junctions between grains (Brunet et al., 2008; Guyer & Johnson, 1999, 2009; Jia et al., 2011; P.
40 A. Johnson & Jia, 2005; Langlois & Jia, 2014; Renaud et al., 2012; Rivière et al., 2015).

41 Previous work suggests that the nonlinear elastic response of consolidated granular media like
42 rocks arises from two distinct mechanisms, one that might be related to the opening/closing of
43 grain contacts, and the other one related to the shearing of grain junctions (Renaud et al., 2012;
44 Rivière et al., 2015). To confirm this hypothesis and better understand the underlying physics,
45 we seek to investigate the nonlinear elastic response of materials simpler than rocks, both in
46 terms of composition and microstructural features. In our previous work (Gao et al., 2022), we
47 studied the influence of relative humidity (RH) on the nonlinear elastic properties of glass bead
48 samples. We found that all extracted nonlinear parameters increase with RH. If indeed both
49 mechanisms exist, this suggests that they are affected similarly in glass beads and cannot be
50 distinguished using changes in RH. In this study, we further attempt to distinguish both
51 mechanisms, by investigating the role of grain shape on the nonlinear elastic properties of
52 granular media. To do so, we use a technique called Dynamic Acousto-Elastic Testing (DAET),
53 a pump-probe approach that allows one to retrieve the full nonlinear elastodynamic response of
54 materials including hysteresis and transient weakening (Renaud et al., 2009, 2011). We carry out
55 DAET measurements on samples of spherical glass beads and angular sand at various RH
56 conditions, and hypothesize that shearing of grain junctions in samples composed of angular
57 grains is more hindered than in samples made of spherical grains.

58

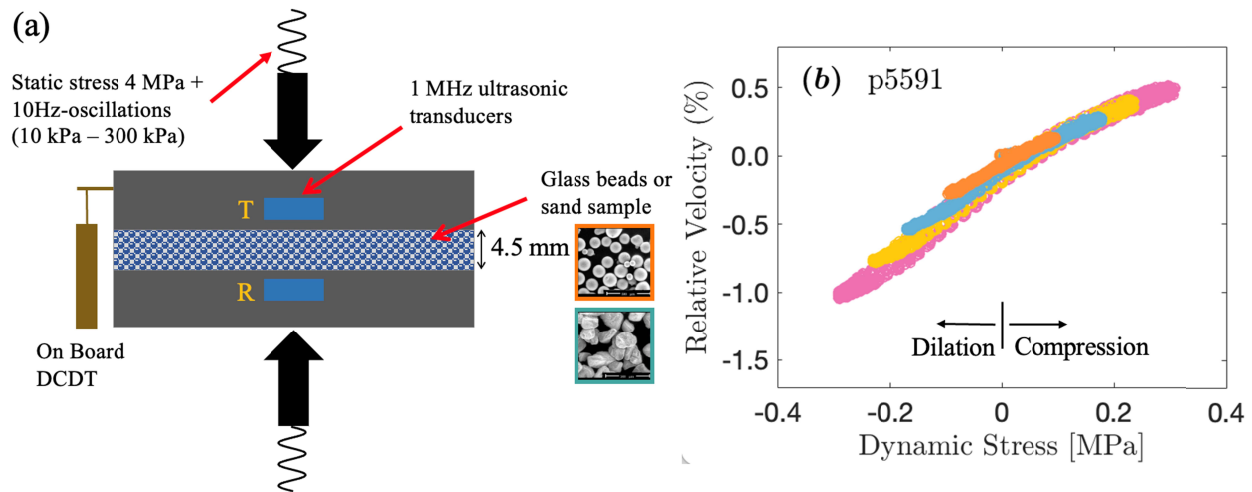
59 **2 Materials and Methods**

60 We prepare samples of spherical soda-lime glass beads (diameter 100-140 μm , Mo-Sci
61 Corporation, Rolla, Missouri) and angular, fine quartz sand (diameter 50-150 μm , 99.8% SiO₂
62 with minor amounts of Fe₂O₃, Al₂O₃, <0.1% each, U.S. Silica Company) using a setup identical
63 to our previous study (Gao et al., 2022). We place a 4.5 mm thick pack of granular media (i.e.,
64 glass beads or sand) on top of a steel block of area 10*10 cm². The sample is left overnight in a
65 sealed bag with either desiccant or a 100% RH humid environment, for dry (~10% RH) and
66 humid (100% RH) samples, respectively. The sample is then quickly taken out of the sealed bag
67 and a second steel block of identical size is placed on top of the granular layer. The sides are
68 sealed using multiple layers of tape. Two P-wave sensors with a central frequency of 1 MHz

69 (2.54 cm in diameter, V102-RM from Olympus, Waltham, MA) are placed at the bottom of blind
 70 holes inside the steel blocks – with a thin layer of molasses to ensure proper ultrasonic coupling
 71 – to track changes in elastic state. The sample assembly is then placed inside a loading apparatus.
 72 An on-board direct current displacement transducer (DCDT) is attached to the top steel block
 73 and referenced to the base of the loading apparatus to track thickness changes. A load cell is also
 74 placed in series between the sample and the hydraulic ram to measure force/stress. In addition to
 75 the eight experiments conducted with glass beads (reported in Gao et al., 2022), a total of
 76 fourteen experiments are conducted in sand, that is 22 experiments total.

77 A static stress of 4MPa is first applied to the sample with a hydraulic ram and maintained
 78 constant throughout the experiment via servocontrol. Dynamic oscillations are then super-
 79 imposed to the static stress, also via servocontrol. We first apply two oscillation sets with 0.3
 80 MPa peak amplitude for initial compaction and homogenization. Then we conduct four identical
 81 DAET oscillation sets with linearly increasing peak amplitudes ranging from 0.01 MPa to 0.3
 82 MPa. Each oscillation set includes 15 oscillations, and each oscillation consists of 50 sinusoidal
 83 cycles at 10 Hz, separated by 20-second hold intervals. Detailed plots of stress and thickness
 84 versus time are shown in Fig. S1.

85



86

87 Figure 1. Experimental setup and typical result. (a) Experimental setup showing the loading
 88 apparatus and sample assembly. (b) Typical nonlinear signature (experiment p5591 is for a sand
 89 sample at 100% RH). Only 4 out of 15 dynamic stress levels are shown for clarity. The
 90 signatures for all 22 samples are shown in Figs. S4-5.

91

92 3 Data Analysis

93 After applying static stress to the sample, we measure the initial layer thickness with a caliper.
 94 We hand-pick the first arrival of a reference waveform (average of 50 consecutive waveforms
 95 taken after applying static stress) to estimate the initial time-of-flight. We then use thickness
 96 changes Δh measured with the displacement sensor and time-of-flight changes Δt estimated using

97 cross-correlation to calculate the wave velocity c throughout the experiment (Gao et al., 2022).
 98 Next, we compute the relative wave velocity change $\Delta c/c$ for each oscillation using $\Delta c/c =$
 99 $(c_{osc} - c_0)/c_0$, where c_0 represents the pre-oscillation wave velocity, and c_{osc} represents the
 100 wave velocity during the oscillation (Fig. S2). We can then generate the so-called nonlinear
 101 signatures by plotting relative velocity change $\Delta c/c$ as a function of dynamic stress (Fig. 1b).

102 To help us quantify the amount and type of elastic nonlinearity, we project the $\Delta c/c$ vs time
 103 signals onto a basis of sine and cosine functions at multiples (0, 1, 2) of the oscillation frequency
 104 (10 Hz). We then extract the magnitude of the harmonics R_n where $n = 0, 1, 2$. Using n up to 2
 105 is shown to be sufficient to capture the complexity of the nonlinear signatures (Gao et al., 2022).
 106 The parameter R_0 characterizes the transient, average weakening occurring during the dynamic
 107 disturbance, while parameters R_1 and R_2 correspond approximately to the slope and curvature of
 108 the nonlinear signatures, respectively (Fig. S3). After obtaining the coefficients R_n , the dynamic
 109 stress dependence can be considered using the general formulation:

$$110 \quad R_n = a_n \sigma^{\nu_n} \quad (1)$$

111 where, for a fixed n , a particular ν -value represents a particular type of nonlinearity (and
 112 associated physical mechanism), and the variable a represents how much of this mechanism or
 113 nonlinearity type is present in the sample. Taking logarithm (base 10) on both sides, Eq. 1 can be
 114 written as:

$$115 \quad \log(R_n) = \nu_n \log(\sigma) + \log(a_n) \quad (2)$$

116 Plotting $\log(R_n)$ vs. $\log(\sigma)$, the slope ν_n tells us about the nonlinearity type, and the y-intercept
 117 ($\log(a_n)$) indicates how much nonlinearity is present.

118

119 **4 Results and Discussion**

120 Typical nonlinear signatures at four dynamic stress amplitudes are shown in Fig. 1b. Similar
 121 plots for the 22 samples are shown in Figs. S4-5. They all exhibit a similar positive correlation
 122 between wave velocity and dynamic stress, where as expected, the wave velocity is larger when
 123 dynamic stress is positive (compression phase), and smaller when dynamic stress is negative
 124 (dilation phase). We also observe that the slopes of the signature (R_1 component) dominate
 125 compared to the offset (R_0 component) and curvature (R_2 component), which is typical when
 126 pump and probe are aligned (vertical direction here, see Fig. 1a) (Renaud et al., 2013). Some
 127 rather large hysteresis can be observed for some of the samples, irrespective of RH level or grain
 128 shape. The reason behind the variability in hysteresis size is not clear and additional work would
 129 be required. Finally, we observe that for some samples, the slope appears larger during the
 130 dilation phase than during compression, suggesting that during the compression phase, the grain
 131 junctions are more tightly closed, producing smaller velocity changes (Figs. S4-5).

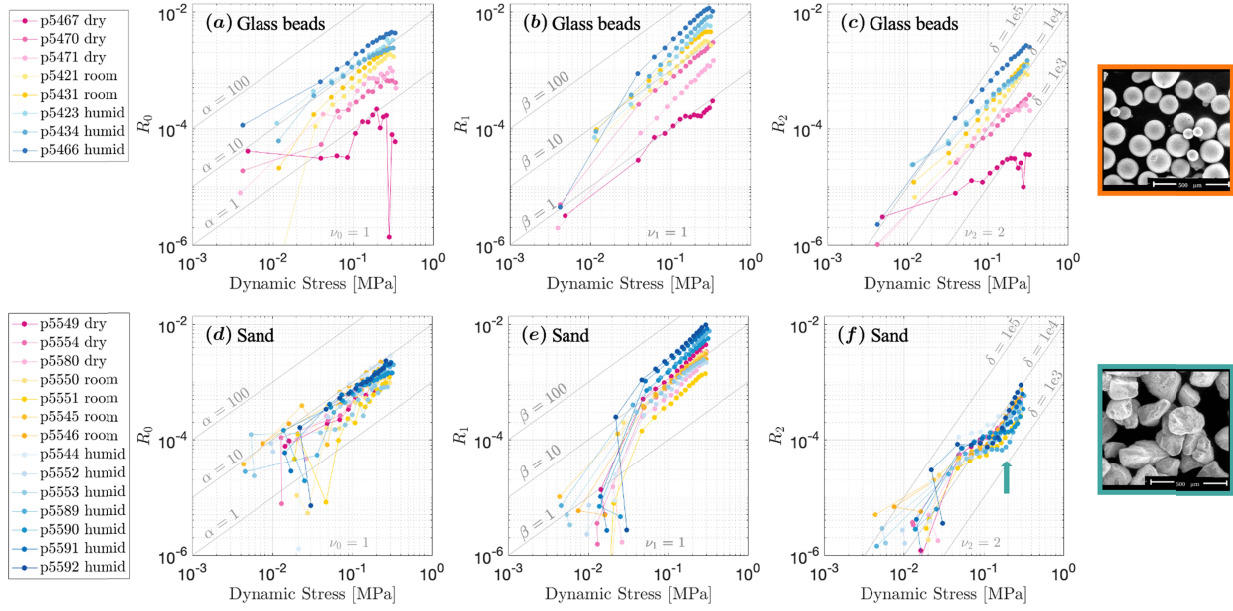
132 To obtain a quantitative assessment of the effect of grain shape and RH, we extract the harmonic
 133 content of all signatures. We calculate the Fourier series coefficients from the $\Delta c/c$ vs time
 134 signals at frequencies nf where f is the pump frequency (10 Hz) and $n = 0, 1, 2$. These
 135 coefficients, called R_n and representing the harmonic content, are shown in Fig. 2. The

136 harmonics are shown as a function of peak dynamic stress amplitude for both glass bead and
 137 sand samples, and under dry (~10%), humid (100%) as well as room humidity (~60%)
 138 conditions. On these log-log plots, following Eq. 2, the slope ν_n informs us about the
 139 nonlinearity type and the y-intercept ($\log(a_n)$) indicates how much nonlinearity is present. We
 140 see that in glass beads, the R_n values are larger in fully humid samples than in drier samples,
 141 while in sand, all the curves seem to overlap, that is, the nonlinearity level seems rather
 142 independent of RH. For both sample types, the R_0 and R_1 values fit roughly linearly ($\nu_0 \approx 1$,
 143 $\nu_1 \approx 1$) with dynamic stress amplitude. Such scalings for R_0 and R_1 suggest that the y-intercepts
 144 on these plots correspond to the hysteretic and quadratic nonlinear parameters α and β ,
 145 respectively. As for the R_2 values, they scale roughly quadratically ($\nu_2 \approx 2$), which suggest that
 146 the y-intercept correspond to the cubic nonlinear parameter δ . Note that for sand, R_2 is rather
 147 stress-independent at low stress and starts to increase quadratically only above ~0.1-0.2 MPa (as
 148 indicated by the small vertical arrow in Fig. 2f). Based on these scalings, we overlay parallel
 149 lines to indicate the value of each nonlinear parameter for a given y-intercept. The three
 150 nonlinear parameters α , β and δ dictate the strain-dependence of the elastic modulus M (or
 151 equivalently the wave velocity c) according to:

$$\frac{\Delta M}{M_0} = 2 \frac{\Delta c}{c_0} = \beta \varepsilon + \delta \varepsilon^2 + \alpha(\varepsilon_0 + \text{sign}(\dot{\varepsilon})\varepsilon)$$

152 where ε is the dynamic strain, $\dot{\varepsilon}$ is the strain rate, and ε_0 is the dynamic strain amplitude.
 153 Because our controlling variable is stress rather than strain, we convert from strain to stress
 154 assuming that the nonlinearity is small, i.e., $\sigma = M_0 \varepsilon$, where $M_0 = 1$ GPa which corresponds to
 155 an average linear elastic modulus for all samples. This allows us to compare the nonlinear
 156 parameters with values found in the existing literature where, most of the time, the controlling
 157 variable is strain (Guyer & Johnson, 2009).

158 Harmonic amplitude plots, sorted per samples rather than R_n values, are also included in the
 159 supplementary materials (Figs. S6-7). For both sample types, at a given dynamic stress
 160 amplitude, we find that R_1 is larger than R_0 and R_2 , which is consistent with our previous
 161 observation that the slope dominates the nonlinear signatures compared to the offset and the
 162 curvature.

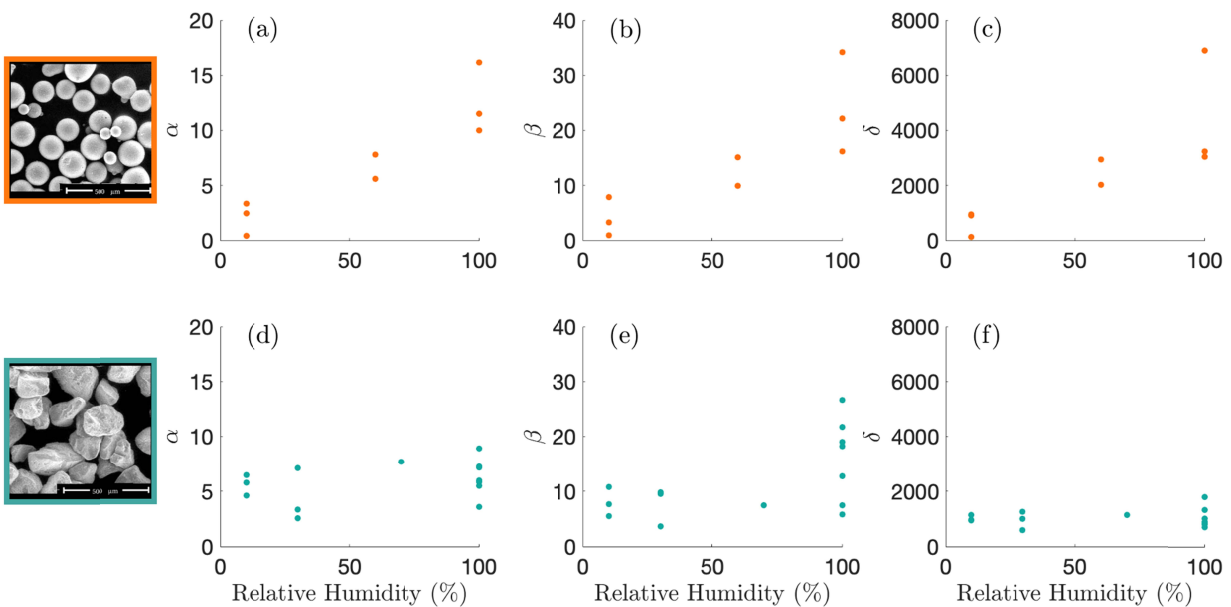


163

164 Figure 2. Harmonic amplitudes R_n as a function of dynamic stress amplitude for all glass beads
 165 (top row) and sand (bottom row) samples. Only results from the third DAET test are shown for
 166 clarity. (a-d) Parameter R_0 . The overall scaling is linear [$\nu_0 \approx 1$ in Eq. (2)]. (b-e) Parameter R_1 .
 167 The overall scaling is roughly linear [$\nu_1 \approx 1$ in Eq. (2)]. (c-f) Parameter R_2 . The scaling is
 168 roughly quadratic [$\nu_2 \approx 2$ in Eq. (2)]. Note the kink in the curves at ~ 0.2 MPa for the sand
 169 samples – panel f – as pointed out by the small vertical arrow (also see Fig. 4).

170 We plot the extracted nonlinear parameters α , β , and δ for glass beads and sand samples as a
 171 function of RH level in Fig. 3. We find that overall, both materials have a similar range of elastic
 172 nonlinearity. However, while all nonlinear parameters increase with RH for glass beads, little
 173 variation can be seen in sand. For sand, α and δ exhibit no variation with RH, and only a small
 174 increase in β for fully humid samples, on average, although scatter is quite large. We do not
 175 know if this increase in β at 100% is real or due to the large scatter; we conducted more
 176 experiments at 100% RH than at drier conditions, so the scatter might appear larger for that
 177 reason. We are currently designing a new setup where a single sample kept under static load can
 178 be monitored while being humidified/dried. By doing so, we anticipate reducing uncertainties by
 179 monitoring the elastic nonlinearity of a single sample instead of different samples.

180

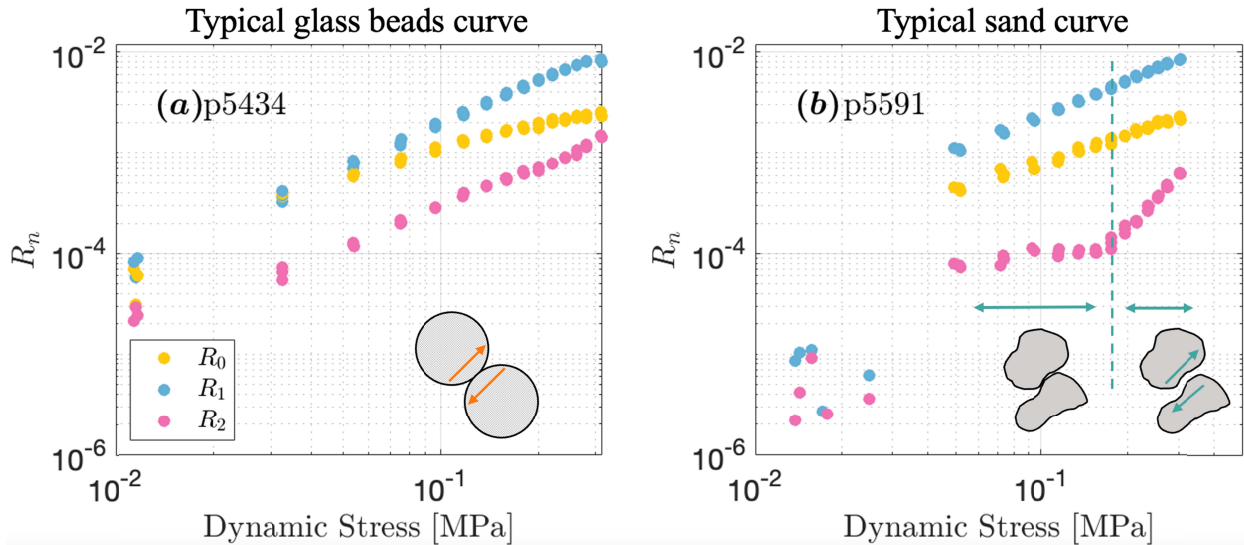


181

182 Figure 3. Nonlinear parameters as a function of RH for glass beads (top row) and sand (bottom
 183 row). These parameters are related to a_n in Eq. (2), that is, (a)(d) α related to a_0 , (b)(e) β related
 184 to a_1 , and (c)(f) δ related to a_2 . Each point represents one DAET test (four tests per experiment).
 185 While all nonlinear parameters increase with RH for glass beads, they seem rather independent
 186 of RH in sand.

187 As discussed in the introduction, previous studies (Renaud et al., 2012; Rivière et al., 2015,
 188 2016) suggest that there exists two main physical mechanisms behind the nonlinear elastic
 189 properties of granular/damaged solids: the parameter β , (related to R_1) that is likely related to the
 190 opening/closing of mesoscopic features such as cracks and grain-grain junctions, while all other
 191 parameters (α , related to R_0 ; δ , related to R_2 as well as hysteresis area (Rivière et al., 2015)
 192 might be related to shearing/sliding/partial slip of these same features. In this work, we find that
 193 the nonlinear parameters are rather independent of RH in sand, while showing a large
 194 dependence of RH in glass beads. This is in line with the interpretation made in our previous
 195 study (Gao et al., 2022), hypothesizing that adsorbed water on glass beads pushes the beads apart
 196 (similar to a small increase in pore pressure (Gor & Gurevich, 2018; Gor & Neimark, 2010),

197 making the junctions weaker and more nonlinear. The fact that the elastic nonlinearity does not
 198 significantly change with RH in sand might come from grain interlocking, that is, the angular
 199 grains prevent adsorbed water from weakening/dilating the sample. Previous results in porous
 200 sandstones have shown that adsorbed water on the grains causes tensile deformation and reduced
 201 elastic moduli (Amberg & McIntosh, 1952; Guyer & Kim, 2015; Yurikov et al., 2018), although
 202 the grains are angular. This is in contradiction with our results in unconsolidated sand, where
 203 changes in RH have little effect, but seems to suggest that in sandstones, the changes in RH
 204 affect the soft bonds between the grains, rather the bare contacts between grains.



205

206 Figure 4. Harmonic amplitudes extracted from the nonlinear signatures on a log-log scale. The
 207 parameter R_0 represents the transient elastic weakening, while R_1 and R_2 represent the slope and
 208 curvature of the nonlinear signatures. Only the data from DAET oscillation set No. 2, 3, and 4
 209 are shown due to the possible large compaction during the first DAET oscillation set. (a) A
 210 typical glass bead sample at 100% RH (b) A typical sand sample at 100% RH.

211 Finally, we emphasize our previous observation that in sand samples, the parameter R_2 is stress-
 212 independent at low dynamic stress amplitudes and starts to increase quadratically for amplitudes
 213 larger than ~ 0.1 – 0.2 MPa (small arrow in Fig. 3f). In Fig. 4, we show the R_n values vs dynamic
 214 stress amplitude for one typical glass bead sample (Fig. 4a) and one typical sand sample (Fig.
 215 4b). We see a clear kink in the curve for R_2 in sand, while it increases monotonically with stress
 216 amplitude in glass beads. If R_2 , related to the curvature of the nonlinear signatures and the
 217 parameter δ , originates from shearing/partial slip of the grain junctions – as we argue – then this
 218 suggests that shearing/partial slip is mostly absent at low stress/strain amplitudes due to grain
 219 locking, and starts taking place only above a particular stress amplitude (~ 0.1 – 0.2 MPa here). In
 220 comparison, shearing/partial slip in spherical glass beads likely initiates at much lower dynamic
 221 stress/strain amplitudes. Another interesting observation is that other R_n values in sand do not
 222 exhibit any such amplitude threshold. Because previous work suggests that β/R_1 is related to
 223 one mechanism while all other parameters are related to a second mechanism, we could have

224 expected both R_0 and R_2 to exhibit an amplitude threshold. This is the not the case and further
225 work would be needed to investigate this discrepancy.

226

227 **5 Conclusions**

228 In this study, we investigate the effect of grain shape and relative humidity on the nonlinear
229 elastic properties of granular media by conducting experiments on spherical glass beads and
230 angular quartz sand. We found that, compared to glass beads, the elastic nonlinearity of angular
231 sand does not increase significantly with RH, but is rather independent of RH, which we attribute
232 to grain interlocking that prevents adsorbed water from weakening the grain junctions.
233 Furthermore, for one of the nonlinear parameters (δ/R_2) which has been attributed to
234 sliding/partial slip of grain junctions, we observe a sharp amplitude threshold in sand but not in
235 glass beads. This seems to confirm that this nonlinear parameter (δ/R_2) is indeed related to
236 sliding/partial slip of the grain junctions. Below the amplitude threshold, i.e., at low dynamic
237 stress oscillations, the angular grains of sand are locked, and no sliding/partial slip can occur.
238 This mechanism seems to get activated only at larger stress oscillations when the grain junctions
239 unlock.

240

241 **Acknowledgments**

242 The authors would like to thank Chris Marone for his help with the loading apparatus and many
243 helpful discussions, Steve Swavelly for technical support, and David C. Bolton, Srisharan
244 Shreedharan, Clay Wood, Samson Marty, and Raphael Affinito for their help with operating the
245 loading apparatus. This work was partially supported by a grant from the U.S. Department of
246 Energy, Office of Basic Energy Sciences (Award Number DE-SC0017585) to PS, and a grant
247 from the U.S. Department of Energy, Office of Basic Energy Sciences (Award Number DE-
248 SC0022842) to JR.

249

250 **Open Research**

251 The data and code used in the study are available at Penn State University's Scholar Sphere via
252 [doi:10.26207/ppqc-7d70, [https://scholarsphere.psu.edu/resources/0d041b4d-57c9-457c-9525-](https://scholarsphere.psu.edu/resources/0d041b4d-57c9-457c-9525-a7282c63e5f8)
253 [a7282c63e5f8](https://scholarsphere.psu.edu/resources/0d041b4d-57c9-457c-9525-a7282c63e5f8)] with all rights reserved.

254

255

256

257

258

259

260

261

262

263

264

265
266
267
268

References

- 269 Abeele, K. V. D., & De Visscher, J. (2000). Damage assessment in reinforced concrete using
270 spectral and temporal nonlinear vibration techniques. *Cement and Concrete Research*,
271 30(9), 1453–1464. [https://doi.org/10.1016/S0008-8846\(00\)00329-X](https://doi.org/10.1016/S0008-8846(00)00329-X)
- 272 Abeele, K. V. D., Carmeliet, J., Johnson, P. A., & Zinszner, B. (2002). Influence of water
273 saturation on the nonlinear elastic mesoscopic response in Earth materials and the
274 implications to the mechanism of nonlinearity. *Journal of Geophysical Research: Solid*
275 *Earth*, 107(B6), ECV 4-1-ECV 4-11. <https://doi.org/10.1029/2001JB000368>
- 276 Amberg, C. H., & McIntosh, R. (1952). A study of adsorption hysteresis by means of length
277 changes of a rod of porous glass. *Canadian Journal of Chemistry*, 30(12), 1012–1032.
278 <https://doi.org/10.1139/v52-121>
- 279 Astorga, A., Guéguen, P., & Kashima, T. (2018). Nonlinear Elasticity Observed in Buildings
280 during a Long Sequence of Earthquakes. *Bulletin of the Seismological Society of*
281 *America*, 108(3A), 1185–1198. <https://doi.org/10.1785/0120170289>
- 282 Bittner, J. A., & Popovics, J. S. (2022). Transient nonlinear vibration characterization of building
283 materials in sequential impact scale experiments. *Frontiers in Built Environment*, 8,
284 949484. <https://doi.org/10.3389/fbuil.2022.949484>
- 285 Breazeale, M. A., & Ford, J. (1965). Ultrasonic Studies of the Nonlinear Behavior of Solids.
286 *Journal of Applied Physics*, 36(11), 3486–3490. <https://doi.org/10.1063/1.1703023>
- 287 Brunet, T., Jia, X., & Johnson, P. A. (2008). Transitional nonlinear elastic behaviour in dense
288 granular media. *Geophysical Research Letters*, 35(19).
289 <https://doi.org/10.1029/2008GL035264>

- 290 Buck, O., Morris, W. L., & Richardson, J. M. (1978). Acoustic harmonic generation at unbonded
291 interfaces and fatigue cracks. *Applied Physics Letters*, *33*(5), 371–373.
292 <https://doi.org/10.1063/1.90399>
- 293 Delorey, A. A., Guyer, R. A., Bokelmann, G. H. R., & Johnson, P. A. (2021). Probing the
294 Damage Zone at Parkfield. *Geophysical Research Letters*, *48*(13), e2021GL093518.
295 <https://doi.org/10.1029/2021GL093518>
- 296 Feng, X., Fehler, M., Brown, S., Szabo, T. L., & Burns, D. (2018). Short-Period Nonlinear
297 Viscoelastic Memory of Rocks Revealed by Copropagating Longitudinal Acoustic
298 Waves. *Journal of Geophysical Research: Solid Earth*, *123*(5), 3993–4006.
299 <https://doi.org/10.1029/2017JB015012>
- 300 Feng, X., Fehler, M., Burns, D., Brown, S., & Szabo, T. L. (2022). Effects of humidity and
301 temperature on the non-linear elasticity of rocks. *Geophysical Journal International*,
302 *231*(3), 1823–1832. <https://doi.org/10.1093/gji/ggac292>
- 303 Gao, L., Shokouhi, P., & Rivière, J. (2022). Effect of relative humidity on the nonlinear elastic
304 response of granular media. *Journal of Applied Physics*, *131*(5), 055101.
305 <https://doi.org/10.1063/5.0073967>
- 306 Gor, G. Y., & Gurevich, B. (2018). Gassmann Theory Applies to Nanoporous Media.
307 *Geophysical Research Letters*, *45*(1), 146–155. <https://doi.org/10.1002/2017GL075321>
- 308 Gor, G. Y., & Neimark, A. V. (2010). Adsorption-Induced Deformation of Mesoporous Solids.
309 *Langmuir*, *26*(16), 13021–13027. <https://doi.org/10.1021/la1019247>
- 310 Guyer, R. A., & Johnson, P. A. (1999). Nonlinear Mesoscopic Elasticity: Evidence for a New
311 Class of Materials. *Physics Today*, *52*(4), 30–36. <https://doi.org/10.1063/1.882648>

- 312 Guyer, R. A., & Johnson, P. A. (2009). *Nonlinear Mesoscopic Elasticity*. Weinheim, Germany:
313 Wiley-VCH Verlag GmbH & Co. KGaA. <https://doi.org/10.1002/9783527628261>
- 314 Guyer, R. A., & Kim, H. A. (2015). Theoretical model for fluid-solid coupling in porous
315 materials. *Physical Review E*, *91*(4), 042406.
316 <https://doi.org/10.1103/PhysRevE.91.042406>
- 317 Hillers, G., Retailleau, L., Campillo, M., Inbal, A., Ampuero, J.-P., & Nishimura, T. (2015). In
318 situ observations of velocity changes in response to tidal deformation from analysis of the
319 high-frequency ambient wavefield. *Journal of Geophysical Research: Solid Earth*,
320 *120*(1), 210–225. <https://doi.org/10.1002/2014JB011318>
- 321 Jia, X., Brunet, Th., & Laurent, J. (2011). Elastic weakening of a dense granular pack by acoustic
322 fluidization: Slipping, compaction, and aging. *Physical Review E*, *84*(2), 020301.
323 <https://doi.org/10.1103/PhysRevE.84.020301>
- 324 Jin, J., Johnson, P. A., & Shokouhi, P. (2020). An integrated analytical and experimental study of
325 contact acoustic nonlinearity at rough interfaces of fatigue cracks. *Journal of the*
326 *Mechanics and Physics of Solids*, *135*, 103769.
327 <https://doi.org/10.1016/j.jmps.2019.103769>
- 328 Johnson, P., & Sutin, A. (2005). Slow dynamics and anomalous nonlinear fast dynamics in
329 diverse solids. *The Journal of the Acoustical Society of America*, *117*(1), 124–130.
330 <https://doi.org/10.1121/1.1823351>
- 331 Johnson, P. A., & Jia, X. (2005). Nonlinear dynamics, granular media and dynamic earthquake
332 triggering. *Nature*, *437*(7060), 871–874. <https://doi.org/10.1038/nature04015>

- 333 Kim, G., Kim, J.-Y., Kurtis, K. E., & Jacobs, L. J. (2017). Drying shrinkage in concrete assessed
334 by nonlinear ultrasound. *Cement and Concrete Research*, *92*, 16–20.
335 <https://doi.org/10.1016/j.cemconres.2016.11.010>
- 336 Kim, J.-Y., Jacobs, L. J., Qu, J., & Littles, J. W. (2006). Experimental characterization of fatigue
337 damage in a nickel-base superalloy using nonlinear ultrasonic waves. *The Journal of the*
338 *Acoustical Society of America*, *120*(3), 1266–1273. <https://doi.org/10.1121/1.2221557>
- 339 Lacouture, J.-C., Johnson, P. A., & Cohen-Tenoudji, F. (2003). Study of critical behavior in
340 concrete during curing by application of dynamic linear and nonlinear means. *The*
341 *Journal of the Acoustical Society of America*, *113*(3), 1325–1332.
342 <https://doi.org/10.1121/1.1543927>
- 343 Langlois, V., & Jia, X. (2014). Acoustic probing of elastic behavior and damage in weakly
344 cemented granular media. *Physical Review E*, *89*(2), 023206.
345 <https://doi.org/10.1103/PhysRevE.89.023206>
- 346 Manogharan, P., Wood, C., Marone, C., Elsworth, D., Rivière, J., & Shokouhi, P. (2021).
347 Nonlinear elastodynamic behavior of intact and fractured rock under in-situ stress and
348 saturation conditions. *Journal of the Mechanics and Physics of Solids*, *153*, 104491.
349 <https://doi.org/10.1016/j.jmps.2021.104491>
- 350 Matlack, K. H., Kim, J.-Y., Jacobs, L. J., & Qu, J. (2015). Review of Second Harmonic
351 Generation Measurement Techniques for Material State Determination in Metals. *Journal*
352 *of Nondestructive Evaluation*, *34*(1), 273. <https://doi.org/10.1007/s10921-014-0273-5>
- 353 McCall, K. R., & Guyer, R. A. (1994). Equation of state and wave propagation in hysteretic
354 nonlinear elastic materials. *Journal of Geophysical Research: Solid Earth*, *99*(B12),
355 23887–23897. <https://doi.org/10.1029/94JB01941>

- 356 Ostrovsky, L. A., & Johnson, P. A. (2001). Dynamic nonlinear elasticity in geomaterials. *La*
357 *Rivista Del Nuovo Cimento*, 24(7), 1–46. <https://doi.org/10.1007/BF03548898>
- 358 Payan, C., Ulrich, T. J., Le Bas, P. Y., Saleh, T., & Guimaraes, M. (2014). Quantitative linear
359 and nonlinear resonance inspection techniques and analysis for material characterization:
360 Application to concrete thermal damage. *The Journal of the Acoustical Society of*
361 *America*, 136(2), 537–546. <https://doi.org/10.1121/1.4887451>
- 362 Renaud, G., Callé, S., & Defontaine, M. (2009). Remote dynamic acoustoelastic testing: Elastic
363 and dissipative acoustic nonlinearities measured under hydrostatic tension and
364 compression. *Applied Physics Letters*, 94(1), 011905. <https://doi.org/10.1063/1.3064137>
- 365 Renaud, G., Le Bas, P., Ten Cate, J. A., Ulrich, T. J., Carey, J. W., Han, J., et al. (2011).
366 Dynamic Measures of Elastic Nonlinear (Anelastic) Behavior: Dynamic Acousto-
367 Elasticity Testing (DAET). *AGU Fall Meeting Abstracts*, 51, MR51A-2151.
- 368 Renaud, G., Le Bas, P.-Y., & Johnson, P. A. (2012). Revealing Highly Complex Elastic
369 Nonlinear (anelastic) Behavior of Earth Materials Applying a New Probe: Dynamic
370 Acoustoelastic Testing: A New Probe for Elasticity in Rocks. *Journal of Geophysical*
371 *Research: Solid Earth*, 117(B6). <https://doi.org/10.1029/2011JB009127>
- 372 Renaud, G., Rivière, J., Hauptert, S., & Laugier, P. (2013). Anisotropy of dynamic
373 acoustoelasticity in limestone, influence of conditioning, and comparison with nonlinear
374 resonance spectroscopy. *The Journal of the Acoustical Society of America*, 133(6), 3706–
375 3718. <https://doi.org/10.1121/1.4802909>
- 376 Rivière, J., Shokouhi, P., Guyer, R. A., & Johnson, P. A. (2015). A set of measures for the
377 systematic classification of the nonlinear elastic behavior of disparate rocks. *Journal of*

- 378 *Geophysical Research: Solid Earth*, 120(3), 1587–1604.
379 <https://doi.org/10.1002/2014JB011718>
- 380 Rivière, J., Pimienta, L., Scuderi, M., Candela, T., Shokouhi, P., Fortin, J., et al. (2016).
381 Frequency, pressure, and strain dependence of nonlinear elasticity in Berea Sandstone.
382 *Geophysical Research Letters*, 43(7), 3226–3236. <https://doi.org/10.1002/2016GL068061>
- 383 Shokouhi, P., Rivière, J., Lake, C. R., Le Bas, P.-Y., & Ulrich, T. J. (2017). Dynamic acousto-
384 elastic testing of concrete with a coda-wave probe: comparison with standard linear and
385 nonlinear ultrasonic techniques. *Ultrasonics*, 81, 59–65.
386 <https://doi.org/10.1016/j.ultras.2017.05.010>
- 387 Shokouhi, P., Jin, J., Wood, C., Rivière, J., Madara, B., Elsworth, D., & Marone, C. (2020).
388 Dynamic Stressing of Naturally Fractured Rocks: On the Relation Between Transient
389 Changes in Permeability and Elastic Wave Velocity. *Geophysical Research Letters*,
390 47(1), e2019GL083557. <https://doi.org/10.1029/2019GL083557>
- 391 Tadavani, S. K., Poduska, K. M., & Malcolm, A. E. (2020). A non-linear elastic approach to
392 study the effect of ambient humidity on sandstone. *Journal of Applied Physics*, 128(24),
393 244902. <https://doi.org/10.1063/5.0025936>
- 394 TenCate, J. A., Abeeel, K. V. D., Shankland, T. J., & Johnson, P. A. (1996). Laboratory study of
395 linear and nonlinear elastic pulse propagation in sandstone. *The Journal of the Acoustical*
396 *Society of America*, 100(3), 1383–1391. <https://doi.org/10.1121/1.415985>
- 397 TenCate, J. A., Malcolm, A. E., Feng, X., & Fehler, M. C. (2016). The effect of crack orientation
398 on the nonlinear interaction of a *P* wave with an *S* wave. *Geophysical Research Letters*,
399 43(12), 6146–6152. <https://doi.org/10.1002/2016GL069219>

400 Williams, C., Borigo, C., Rivière, J., Lissenden, C. J., & Shokouhi, P. (2022). Nondestructive
401 Evaluation of Fracture Toughness in 4130 Steel Using Nonlinear Ultrasonic Testing.
402 *Journal of Nondestructive Evaluation*, *41*(1), 13. [https://doi.org/10.1007/s10921-022-](https://doi.org/10.1007/s10921-022-00846-5)
403 [00846-5](https://doi.org/10.1007/s10921-022-00846-5)

404 Yurikov, A., Lebedev, M., Gor, G. Y., & Gurevich, B. (2018). Sorption-Induced Deformation
405 and Elastic Weakening of Bentheim Sandstone. *Journal of Geophysical Research: Solid*
406 *Earth*, *123*(10), 8589–8601. <https://doi.org/10.1029/2018JB016003>

407